AIAA JOURNAL
Vol. 42, No. 5, May 2004

Measurements in the Near Field of a Confined Coaxial Square Jet

S. C. M. Yu,* L. P. Chua,† and X. K. Wang‡
Nanyang Technological University, Singapore 639798, Republic of Singapore

The near field of a confined coaxial square jet configuration has been investigated using a two-component laser Doppler anemometer. Measurements at velocity ratios ($\gamma_u = U_o/U_i$) 0.5, 1.0, and 2.0 with a fixed mean velocity (0.7 m/s) for the inner stream were obtained. Reynolds numbers based on the average velocity of the two coflowing streams U_M and the jet equivalent diameter D_e were ranged from 1.53×10^4 to 4.2×10^4. The streamwise vortices generated at the corners of the inner square nozzles had affected the downstream flow development considerably. The spreading rate at $\gamma_u = 0.5$ was found to be the highest among the three cases investigated and that for respective cases were also higher than their circular counterparts under similar flow conditions. Self-similarity can be attained and is in the order of $\gamma_u = 0.5$, 1.0, and 2.0. The difference can be attributed to the relative strength as well as the sense of rotation for the corner streamwise vortices generated by the inner jet. The downstream developments for various velocity components are presented. Finally, the flow structure at different velocity ratios will be briefly discussed via inviscid vortex dynamics.

Nomenclature

A	=	nozzle exit area, m^2
D	=	nozzle width (for square configuration) or diameter (for circular configuration), m
D_e	=	equivalent diameter, m
H	=	shape factor
Re_M	=	Reynolds number, $U_M D_e/\nu$
t	=	thickness of the inner nozzle at exit, m
U	=	streamwise mean velocity, m/s
U_{CL}	=	centerline velocity, m/s
U_M	=	equivalent jet velocity, m/s
U_{max}	=	maximum streamwise mean velocity in any transverse plane, m/s
u', v'	=	rms value of fluctuations of streamwise and lateral velocity
x, y, z	=	Cartesian coordinate system
x_p	=	length of potential core
y_m	=	distance from the axis to the point where $U = U_{max}$
$y_{0.5}$	=	half-width, the largest distance from the axis to the point where $U = 0.5U_{max}$
γ_u	=	velocity ratio, U_o/U_i
γ_{uc}	=	critical velocity ratio
δ^*	=	displacement thickness estimated at $x/D_i = 0.125$, mm
θ	=	momentum thickness estimated at $x/D_i = 0.125$, mm
ν	=	kinematic viscosity
ω_x	=	streamwise vortex
ω_θ	=	normal vortex in either the y or y-z axes direction

Subscripts

i	=	inner jet (nozzle)
o	=	outer jet (nozzle)

Presented as Paper 2002-0731 at the AIAA 40th Aerospace Sciences Meeting, Reno, NV, 14–17 January 2002; received 26 July 2002; revision received 12 September 2003; accepted for publication 14 October 2003.

*Associate Professor, Thermal and Fluids Engineering Division, School of Mechanical and Production Engineering; mcmyu@ntu.edu.sg.

†Associate Professor, Thermal and Fluids Engineering Division, School of Mechanical and Production Engineering.

‡Graduate Student, Thermal and Fluids Engineering Division, School of Mechanical and Production Engineering. Member AIAA.

I. Introduction

THE flowfield of a coaxial jet is complex, involving interaction between the two coflowing streams (inner and outer or annular) as well as that between the annular stream with the surrounding fluid medium.

Forstall and Shapiro[1] showed that the velocity ratio is the most important variable determining the downstream flow development in a coaxial jet. Champagne and Wygnanski[2] reported that the growth of the jet half-width is insensitive to changes of velocity and area ratios. The length of the annular potential core appears to be independent of the velocity ratio and equals to about eight times the annular nozzle width. However, the length of the inner potential core depends on the velocity ratio as well as the area ratio. Durao and Whitelaw[3] showed that coaxial jets tend to reach a self-preserving state much more rapidly than axisymmetric single jets. The presence of swirl hastens this process further.[4] Buresti et al.[5] provided downstream data on mean axial, mean radial, and rms velocity profiles and shear stresses of a coaxial jet configuration using a laser Doppler anemometer with initial turbulence characteristics typical of industrial applications. Their results are essentially similar to those found by Ko and Au.[6]

Ko and Au[6] conducted hot-wire measurements on a coaxial nozzle at three different velocity ratios of 2.5, 1.67, and 1.15 ($1/\gamma_u$). The mean velocity measurements indicated that the initial region of coaxial jets consists of three separation zones. The initial merging zone starts from the jet exit and ends at the boundary of the outer potential cores. This is followed by the intermediate merging zone from the end of the outer potential core to the position where the mean velocity at the centerline begins to decay. The fully merged zone is defined as where the flow conditions become progressively similar to those of a single jet.

More recently, Rehab et al.[7] and Villeramaux and Rehab[8] investigated the coaxial jets within the regime of $\gamma_u (= U_o/U_i) > 1$ using the method of scalar (concentration) mixing measurements. They showed that the near-field flow structure for $\gamma_u > 1$ is dominated by the annular jet and is strongly dependent on γ_u. Two flow regimes are also identified depending on whether γ_u is larger or smaller than a critical value γ_{uc} (γ_{uc} is about 8.0).

Up until now, investigators have concentrated on coaxial circular jets because they represent the simplest flow configuration. The motivation of the present study is that in recent years numerous researchers have indicated that noncircular nozzles have better mixing characteristics than circular counterparts, for example, Yu and Xu,[9] Quinn,[10] and Gutmark and Grinstein.[11] Therefore, combinations of such nozzles in coaxial configurations can be of practical interest. The present work aims at investigating the use of a square nozzle as a method of enhancing the mixing process between two coflowing streams. This type of shape was selected owing to the following two

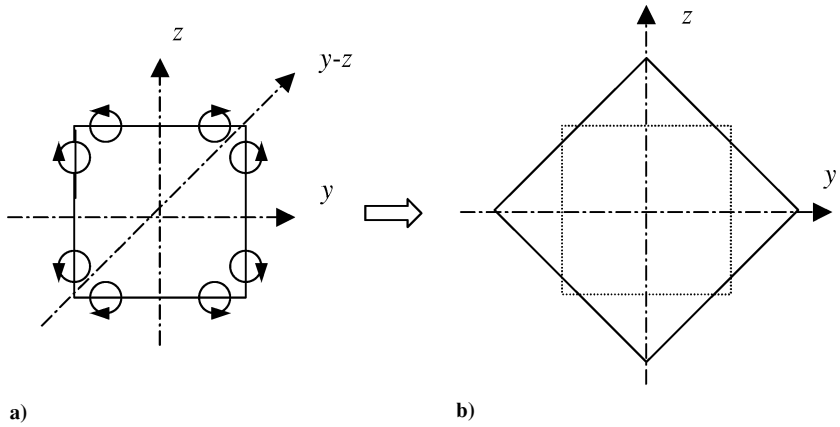

Fig. 1 Sketch of the corner vortices in a square jet and the subsequent axis switching.[12]

considerations. First, square jets belong to noncircular jets that have been the topic of extensive research in the past 15 years (for example, Quinn[10] and Grinstein et al.[12]). The research was motivated mainly by the increased entrainment and enhanced mixing properties relative to those of comparable circular jets. Second, in the absence of aspect-ratio effects the square cross section can be considered as the most regular noncircular shape and the easiest one to be compared with its circular counterpart. Obviously, the azimuthal nonuniformities of the square geometry will add complexities to the flow. It has already been shown that azimuthal nonuniformities will lead to the formation of corner streamwise vortices (see Fig. 1 for illustration). Most of the previous investigations are either focused on $\gamma_u < 1.0$ (e.g., Ko and Au[6] and Au and Ko[13]) or $\gamma_u > 1.0$ (e.g., Durao and Whitelaw[3] and Buresti et al.[5]). It is our interest to have measurements with velocity ratios both greater and less than one using the same test facilities.

Based on our existing knowledge, the only published literature on the coaxial square jet measurements is that of Bitting et al.[14] They conducted visualization and two-color digital particle image velocimetry (DPIV) measurements on three square coaxial nozzles. Three velocity ratios ($\gamma_u^{-1} = 0.15, 0.22,$ and 0.3) were examined, and it has been shown that the internal unmixed region diminished with decreasing velocity ratio. Comparison between circular and square configurations indicated that considerable mixing enhancement can be attained when square nozzles are used. However, their results focused in the very near-field region, that is, $0 \le x/D_o \le 2.5$.

In the present study, in order to obtain a better understanding of the velocity field of a coaxial square jet extensively laser Doppler anemometry (LDA) measurements have been conducted. The interest is concentrated on the near-field region (up to $x/D_i = 34.0$) at three different ratios, that is, $\gamma_u = 0.5$, 1.0, and 2.0. Some global flow characteristics (such as the centerline velocity development, length of inner and outer potential cores, distributions of mean and rms velocities as well as Reynolds shear stresses) at different velocity ratios, as well as some comparisons with available literature on coaxial circular jets, will be presented and discussed.

The following section describes briefly the experimental setup including the laser Doppler anemometer. The results are shown in Sec. III. The paper ends with a summary of important findings.

II. Flow Configuration and Instrumentation

A. Water Tunnel

The experiments were performed in a gravity-driven water facility. The flow is guided by two concentric contractions into the test section. The contractions have equal lengths of 500 mm, with circular shapes at the inlet (inner diameters of 260 and 130 mm, respectively) that smoothly transform into square shapes at the exit plane, as shown in Fig. 2. The inner side widths for the two nozzles are 16 and 32 mm, with the lip thickness at 1 mm. These dimensions contribute an area ratio (outer:inner) $A_o{:}A_i = 2.73$, a value close to most of the previous works, for example, 2.94 of Champagne and Wygnanski,[2] 2.79 of Ko and Au[6] and Au and Ko,[13] and 2.97 of Buresti et al.[5] The area contraction ratios (inlet: exit) for the two nozzles are both at about 45:1, ensuring relatively low turbulence levels (the fluctuations of the streamwise velocity are lower than 2% for both the inner and outer jet) of the jet flows on entering the test section with a cross section of 400×400 mm and 1000 mm in length. The jet exit plane is located at $1D_e$ inside the test section. The four sidewalls were made of Plexiglas® to facilitate optical access. The temperature of the water recycling in the tunnel was kept at 21°C during the course of the experiment. Different velocities of the streams were achieved by incorporating different layers of fine wire meshes upstream of the contraction section. The coordinate system adopted in the present investigation are shown in Figs. 1 and

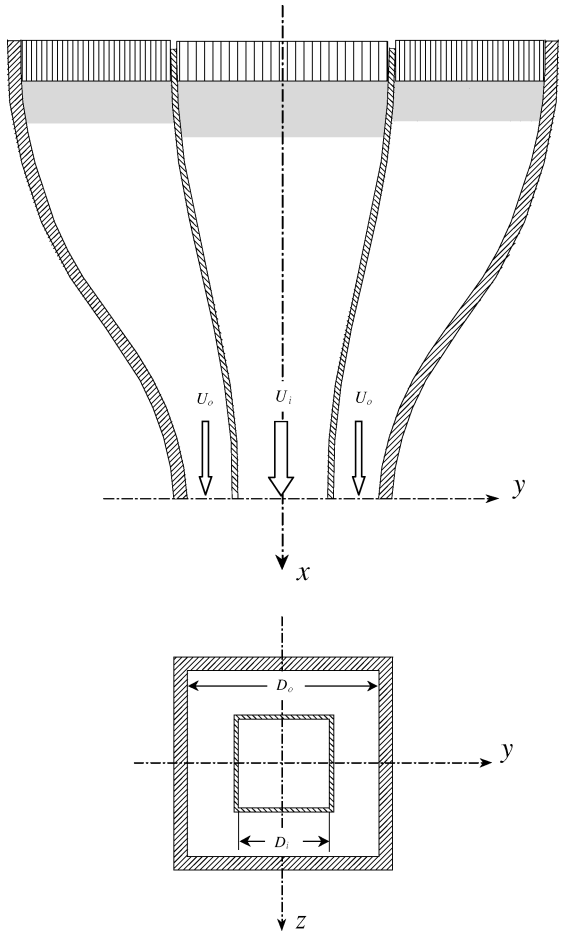

Fig. 2 Schematic of the nozzle configuration.

Table 1 Experimental conditions for the three cases considered

Case	U_i, m/s	U_o, m/s	$\gamma_u = U_o/U_i$	U_M, m/s	$Re_M = U_M D_e/\nu$
1	0.70	0.70	1.0	0.70	2.43×10^4
2	0.70	0.35	0.5	0.443	1.53×10^4
3	0.70	1.40	2.0	1.213	4.20×10^4

2, in which the origin is specified at the center of the jet exit plane and x is along the centerline of the jet (i.e., the main flow direction).

The experimental conditions are given in Table 1. Re_M is the Reynolds number based the equivalent diameter D_e and the equivalent jet velocity U_M in order to have the same momentum flux M as a circular jet, where

$$D_e = \sqrt{\frac{4(A_i + A_o)}{\pi}}, \qquad U_M = \sqrt{\frac{U_i A_i^2 + U_o A_o^2}{A_i + A_o}} \tag{1}$$

During the experiment, U_i was kept constant at 0.70 m/s; and thus the desired velocity ratio $\gamma_u = U_o/U_i$ was achieved by varying the outer velocity U_o only.

B. Laser Doppler Anemometer

A four-beam, two-component fiber-optic LDA manufactured by TSI, Inc., operating in a backward-scatter mode was used to measure the flowfield. A 2-W, argon-ion, water-cooled laser was used to provide a coherent light source for the LDA system. The green (514.5 nm) and blue (488 nm) beams were separated, split, and then transmitted through a 6-m fiberoptic cable to a probe with beam separation 50 mm (TSI Model 9253-350). The probe focused (focusing distance of 350 mm) the four parallel beams to a common point, which formed the measurement volume, whose dimensions were $0.09 \times 0.09 \times 1.3$ mm for the green beams and $0.085 \times 0.085 \times 1.24$ mm for the blue ones. The fringe spacings are 3.72 and 3.52 μm, respectively, for green and blue components. Bragg shifting of frequency up to 500 kHz (on each channel) was used for directional discrimination. By introducing a small amount of seeding particles (titanium dioxide; TiO_2) into the water, a good quality and quantity of Doppler bursts were ensured before acquisition of the LDA data. The Doppler signals were detected by photomultipliers and processed by burst spectrum analyzers (IFA 750 series). The probe was mounted on an automated three-dimensional traversing system with an accuracy of ± 0.01 mm. During the experiment, the axis of the probe was kept normal to the side of the test section to ensure the four beams always intersected on a common point. At each point, a minimum of 3000 Doppler bursts were acquired, which was increased to 5000 in the regions of high turbulence to reduce biasing effects. The accuracy of the normalized mean and rms velocities (normalized by the average velocity of the two coflowing streams) was estimated to be about 2 and 5% and that of Reynolds shear stress less than 10%.

Measurements were taken at various streamwise locations ranging from $x/D_i = 0.125$ up to 34. Stations close to the jet exit had a 31×31 measurement grid (with $\Delta y = 0.06 D_i$ and $\Delta z = 0.06 D_i$), whereas downstream values were obtained from 25×25 measurement grid (with $\Delta y = 0.2 D_i$ and $\Delta z = 0.2 D_i$). The symmetry of the flow about the y and z axes is within 5%.

III. Results and Discussion

A. Jet-Exit Conditions

The mixing characteristics in the near-field region can be substantially affected by the distribution of the velocities at the jet exit. Figure 3 shows the normalized streamwise U/U_i and lateral V/U_i velocities at $x/D_i = 0.125$ for the three velocity ratios. The calculated parameters (displacement thickness, momentum thickness, and the shape factor) show that the boundary layers of the velocity profiles are laminar and the profiles have a top-hat shape (see Table 2 for a summary).

For $\gamma_u = 0.5$ and Fig. 3a, the outer jet is seen to have a weak mean lateral velocity (>1% U_i) directed toward the jet centerline (positive value) near the edge of the outer nozzle wall at $y/D_i = 0.5$. However,

Table 2 Boundary-layer characteristics at $x/D_i = 0.125$ for the respective cases

γ_u	Inner nozzle (δ^*, θ, H)	Outer nozzle on the other side of the inner nozzle lip (δ^*, θ, H)	Outer nozzle (δ^*, θ, H)
0.5	1.7, 0.65, 2.62	1.7, 0.65, 2.62	1.8, 0.7, 2.57
1.0	1.7, 0.7, 2.43	2.5, 0.95, 2.63	2.5, 0.95, 2.63
2.0	2.3, 0.9, 2.56	1.6, 0.6, 2.67	1.6, 0.6, 2.67

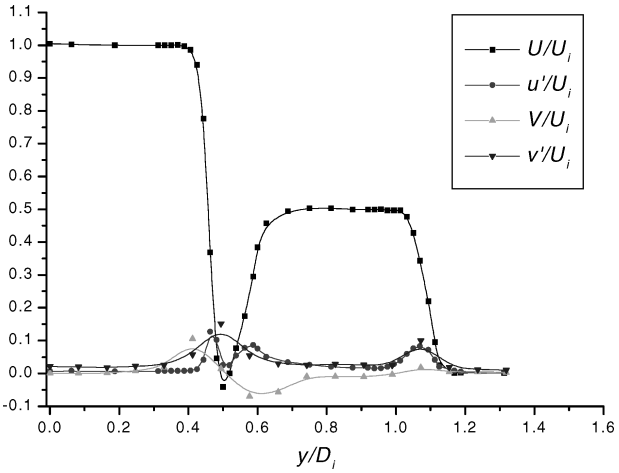

a) $\gamma_u = 0.5$

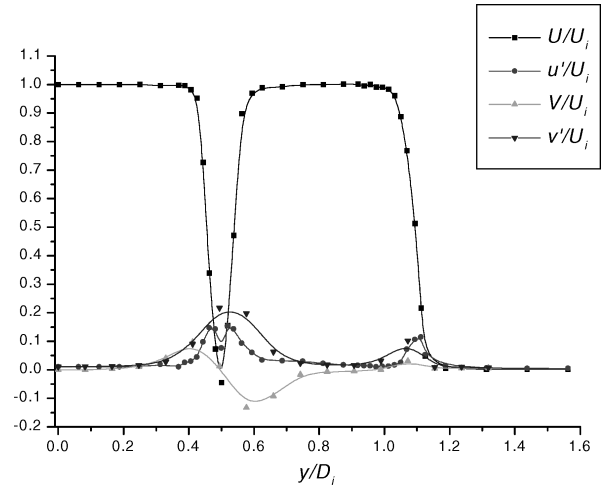

b) $\gamma_u = 1.0$

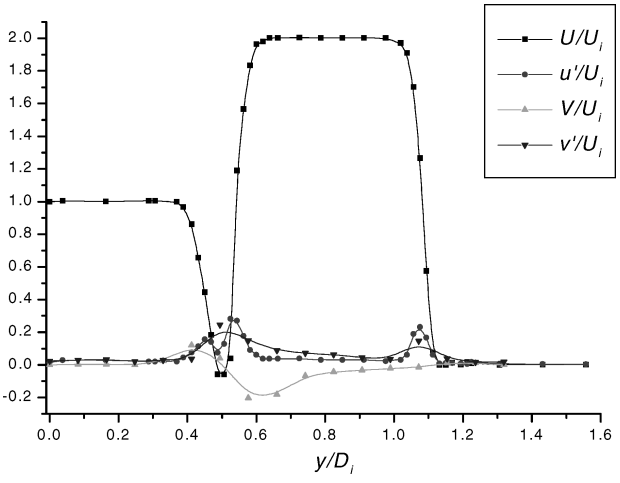

c) $\gamma_u = 2.0$

Fig. 3 Profiles of the streamwise U/U_i and lateral V/U_i mean velocity and the corresponding rms values u'/U_i and v'/U_i at $x/D_i = 0.125$.

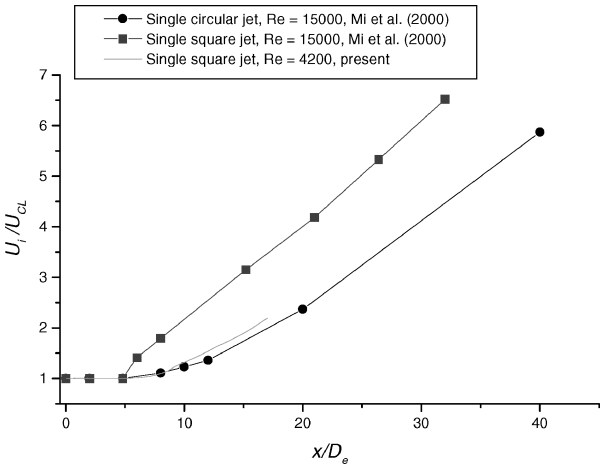

a) Decay of the centerline velocities for a single circular and square jet

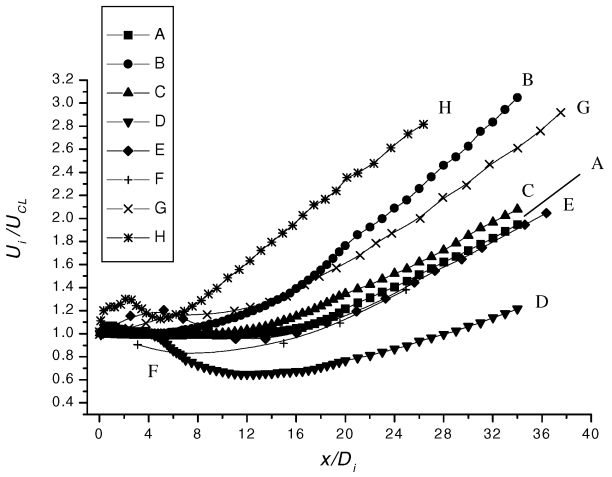

b) Decay of the centerline mean velocity for coaxial square jet at various velocity ratios and comparisons with the results of coaxial circular jets

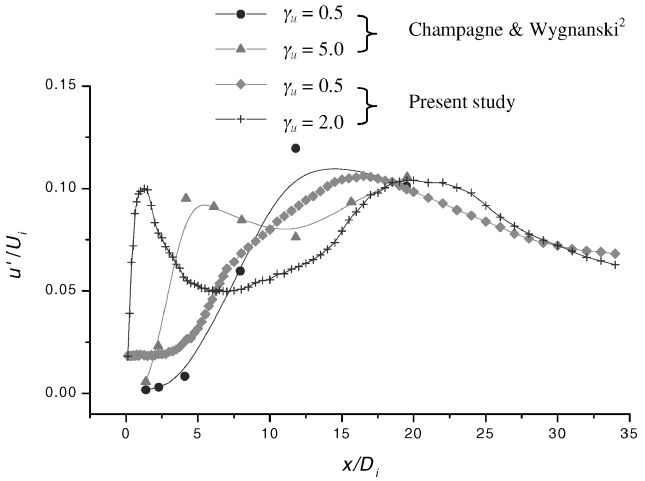

c) Development of the centerline streamwise rms velocities for the two cases $\gamma_u = 2.0$ and 0.5

Fig. 4 Streamwise velocity profiles along the centerline: A, single square jet; B, coaxial square jet, $\gamma_u = 0.5$; C, coaxial square jet, $\gamma_u = 1.0$; D, coaxial square jet, $\gamma_u = 2.0$; E, coaxial circular jet, $\gamma_u = 1.61$, Durao and Whitelaw[3]; F, coaxial circular jet, $\gamma_u = 2.0$, Champagne and Wygnanski[2]; G, coaxial circular jet, $\gamma_u = 1.0$, Ribeiro and Whitelaw[4]; and H, coaxial circular jet, $\gamma_u = 1.0$, swirl number S = 0.26, Ribeiro and Whitelaw.[4]

over most of the inner jet area there are positive lateral velocities tending to spread the jet away from the centerline. In contrast, at $\gamma_u = 2.0$ (Fig. 3c) stronger negative lateral velocity toward the jet centerline is seen to prevail over the whole jet area, which decreases approximately linearly to zero at the centerline. This is compatible with the view that the annular vortex rings grow inwardly to the jet centerline for velocity ratios larger than unity.[11]

Two separated peaks of the streamwise rms velocity can be found at $y/D_i = 0.5$, corresponding to the two boundary layers formed on either side of the nozzle wall, respectively. The maximum rms value in the inner boundary layer is of the order of $0.06U_i$, $0.1U_i$, and $0.18U_i$, for $\gamma_u = 0.5$, 1.0, and 2.0, respectively. The rms level in the inner jet is always at about $0.015U_i$, whereas the rms values within the potential core of the annular jet increase only slightly as γ_u varies from 0.5, 1.0, to 2.0. In addition, with the decrease in velocity ratio γ_u the thickness of the boundary layers on all of the sidewalls of the annular jet increased correspondingly, as expected.

B. Variation of the Centerline Velocities

The decay of the centerline velocity for a single square jet (i.e., when the inner nozzle was removed) is shown in Fig. 4a. The decay rate for the present case is found to be faster than that of a single circular jet but lower than that of another square jet measured by Mi et al.[15] It is obvious that the decay of a square jet is hastened by the presence of the corner vortices[10] compared to its circular counterpart. The jets used by Mi et al.[15] were the orifice types, whereas the present investigation used nozzle jet. The magnitude of secondary velocities generated by the orifice jet would usually be larger than that of nozzle jet, and thus the former would generally have a higher spreading rate.

The results for the coaxial square jet at the three velocity ratios are shown in Fig. 4b. Also shown are the results obtained from the

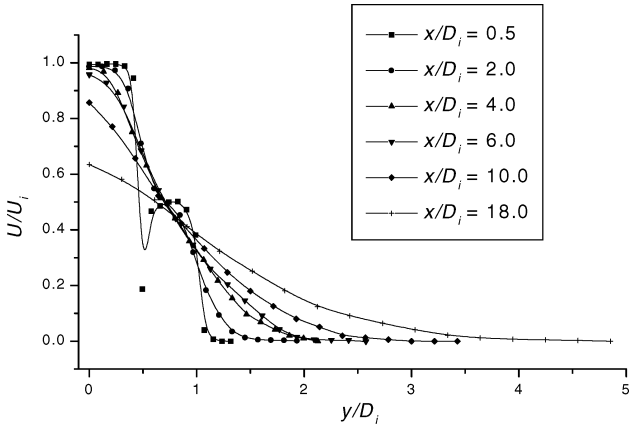

a) U/U_i

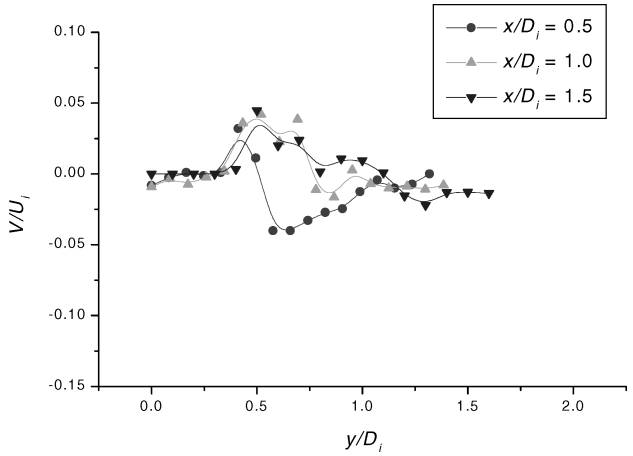

b) V/U_i

Fig. 5 Development of the normalized streamwise U/U_i and lateral V/U_i mean velocity along the y axis for $\gamma_u = 0.5$.

coaxial circular jets by Champagne and Wygnanski,[2] Durao and Whitelaw,[3] and Ribeiro and Whitelaw[4] for comparison purposes. For the case of coaxial square jet, the three cases exhibited similar trends as their circular counterparts: $\gamma_u = 0.5$ has the fastest decay rate and is followed by $\gamma_u = 1.0$ and 2.0. For $\gamma_u = 1.0$, the decay rate for the coaxial square jet is actually faster than its circular counterpart indicating the jet spread is generally assisted by the presence of the corner streamwise vortices. The initial decay rate for $\gamma_u = 0.5$ (up to $x/D_i = 8$) is lower than the case of circular coaxial jet with swirl ($\gamma_u = 1.4$ and swirl no. 0.26). However, as the swirl dissipates gradually with downstream distance the decay rate for the square configuration overtakes and eventually become faster at the end of the near field after $x/D_i = 20$.

Figure 4c shows the development of the centerline streamwise rms velocities for the two cases $\gamma_u = 0.5$ and 2.0. The results obtained by Champagne and Wygnaski[2] are used for comparison. It is obvious that the trend for the two geometries is qualitatively similar. For $\gamma_u = 0.5$, two peaks appeared within the first $25D_i$. The first peak is located just after the end of the potential core whereas the second peak is at the region after the two coflowing streams merged. The two peaks were the direct results from the positive production of the u' components generated by the steep streamwise mean velocity gradients. Similarly for $\gamma_u = 0.5$, the stronger momentum for the inner nozzle delays the production of u' near the centerline until $x/D_i = 15$ as the shear layer generated by the inner nozzle wall diminishes and the velocity profile become more like a single jet.

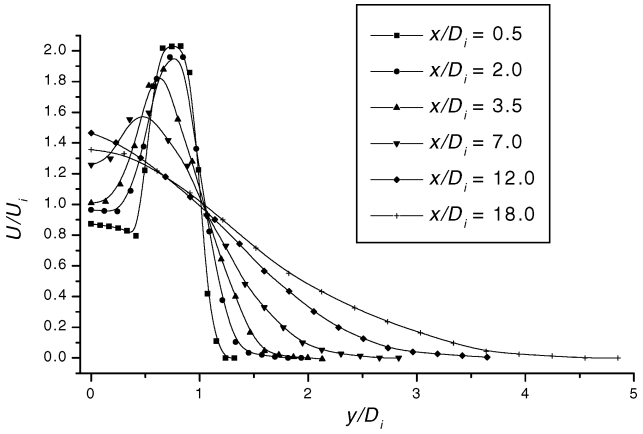

a) U/U_i

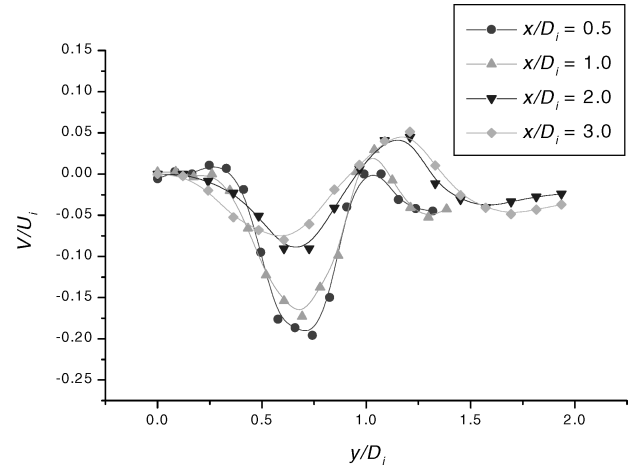

b) V/U_i

Fig. 6 Development of the normalized streamwise U/U_i and lateral V/U_i mean velocity along the y axis for $\gamma_u = 2.0$.

C. Length of the Potential Cores

The lengths of the potential cores for the inner and annular jets along the y axis for respective cases are shown in Table 3. Also shown are the results obtained from circular coaxial jets under similar flow conditions.

The results for $\gamma_u = 2.0$ are similar to the findings of other investigations for coaxial circular jets at $\gamma_u > 1$. The present inner potential core length x_{pi} is approximately $4.0D_i$. Using the formula proposed by Au and Ko[13] where x_{pi} is a function of velocity ratio, the approximate relationship $x_{pi}/D_i \approx 9.9\ U_i/U_o$ (in the range of $0.15 \le U_i/U_o \le 0.8$) provides an estimated value of $x_{pi}/D_i \approx 5.0$ for the present case. The square configuration has a relatively shorter inner potential core than its circular counterpart. For a square jet, the two coflowing streams appear to achieve self-similarity earlier at about $10D_i$ than the results of coaxial circular jets, for example, at about $12D_i$ for Au and Ko[13] and slightly below $12D_i$ for Buresti et al.[5] Similar observations were also found along the diagonal (y–z) axis to within 10–15%.

The end of the outer potential core x_{po} is about $1.75D_i$ for $\gamma_u = 0.5$, and with higher outer velocity the outer potential core length has shown to increase further to $2.5D_i$ and $3.0D_i$ for $\gamma_u = 1.0$ and 2.0, respectively. The result is shorter than the $3.4D_i$ measured by Buresti et al.[5] for $\gamma_u = 1.6$. Our findings are also different from those of Ko

Table 3 Length of the potential cores in terms of inner nozzle diameter D_i for respective cases

U_o/U_i	x_{pi}	x_{po}
$\gamma_u = 0.5$	6	1.75
($\gamma_u = 0.5$; Ref. 11)	(9)	(4.28)
$\gamma_u = 1.0$	9	2.5
$\gamma_u = 2.0$	4	3
($\gamma_u = 1.6$; Ref. 13)	(6.6)	(3.4)

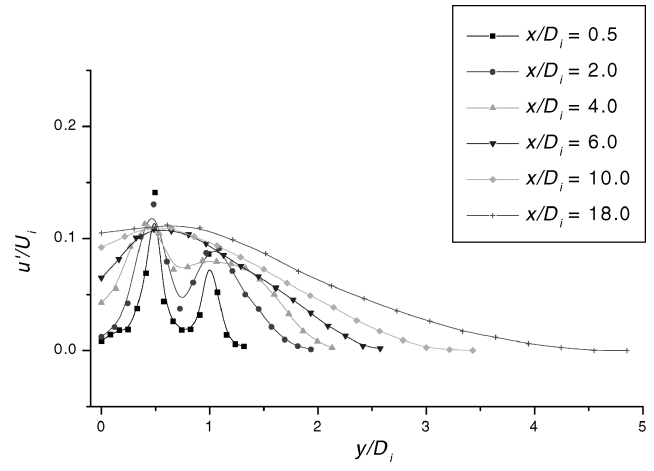

a) Normalized streamwise rms velocity

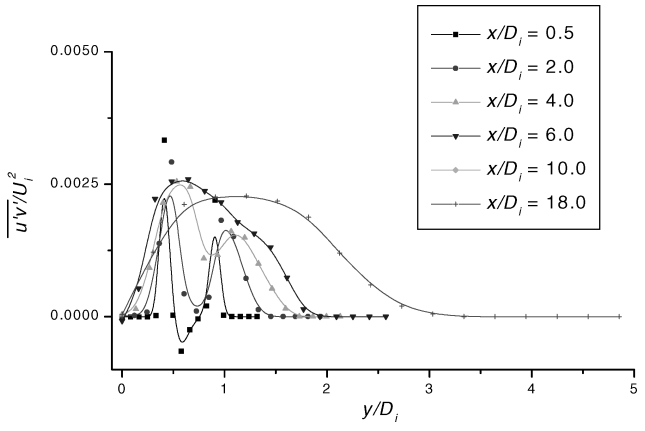

b) Normalized Reynolds shear stress

Fig. 7 Development of the normalized streamwise, lateral, and Reynolds stress for $\gamma_u = 0.5$.

and Au,[6] who showed that x_{po} is a function of the area ratio and almost independent of the velocity ratio. The reason might be because the range of γ_u covered in the present experiment might not be large enough such that the initial boundary layers were relatively thick at the jet exit. As a result, the change of x_{po} becomes more obvious.

D. Downstream Mean Flow Development Along the *y* Axis and *y–z* Axis

Profiles of the normalized streamwise mean velocity U_i/U_o and the corresponding rms streamwise velocity u'/U_i at various streamwise stations are shown in Figs. 5 and 6 for $\gamma_u = 0.5$ and 2.0, respectively.

Immediately behind the jet exit, it can be seen that there are two distinct mixing regions that appear for the three cases as indicated in Figs. 5a and 6a. The wake generated by the inner nozzle wall persisted up to $1.0D_i$ and $0.5D_i$ for $\gamma_u = 0.5$ and 2.0, respectively. For $\gamma_u = 0.5$ (Fig. 5b), relatively stronger lateral velocities existing at around $y/D_i = 0.5$ can be identified and are moving inwardly to the jet axis. Maximum was at about $0.15U_i$ at $x/D_i = 0.5$. For $\gamma_u = 2.0$ and Fig. 6b, the maximum lateral velocity is the highest

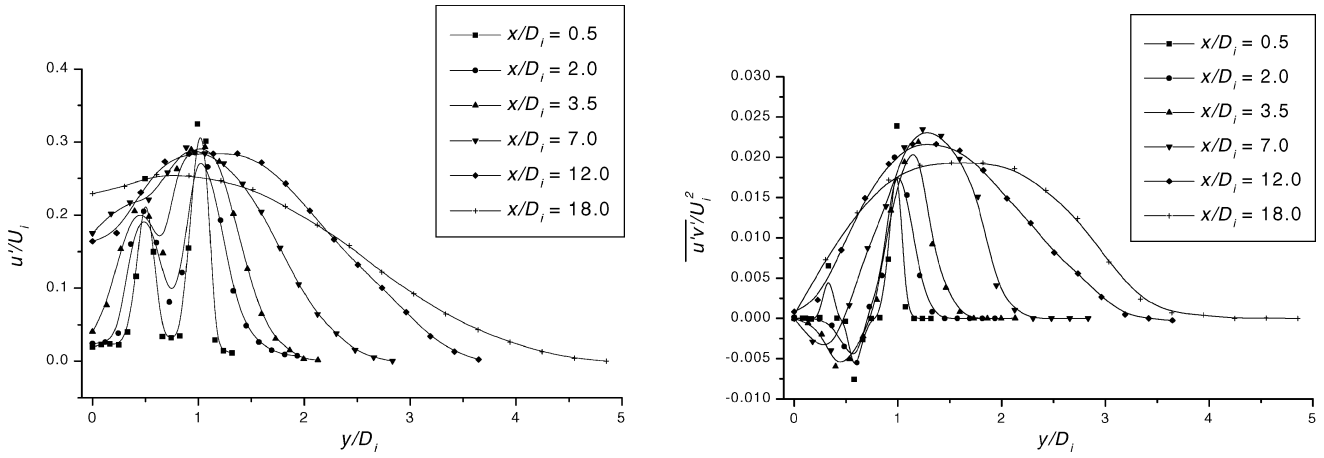

a) Normalized streamwise rms velocity **b) Normalized Reynolds shear stress**

Fig. 8 Development of the normalized streamwise, lateral, and Reynolds stress for $\gamma_u = 2.0$.

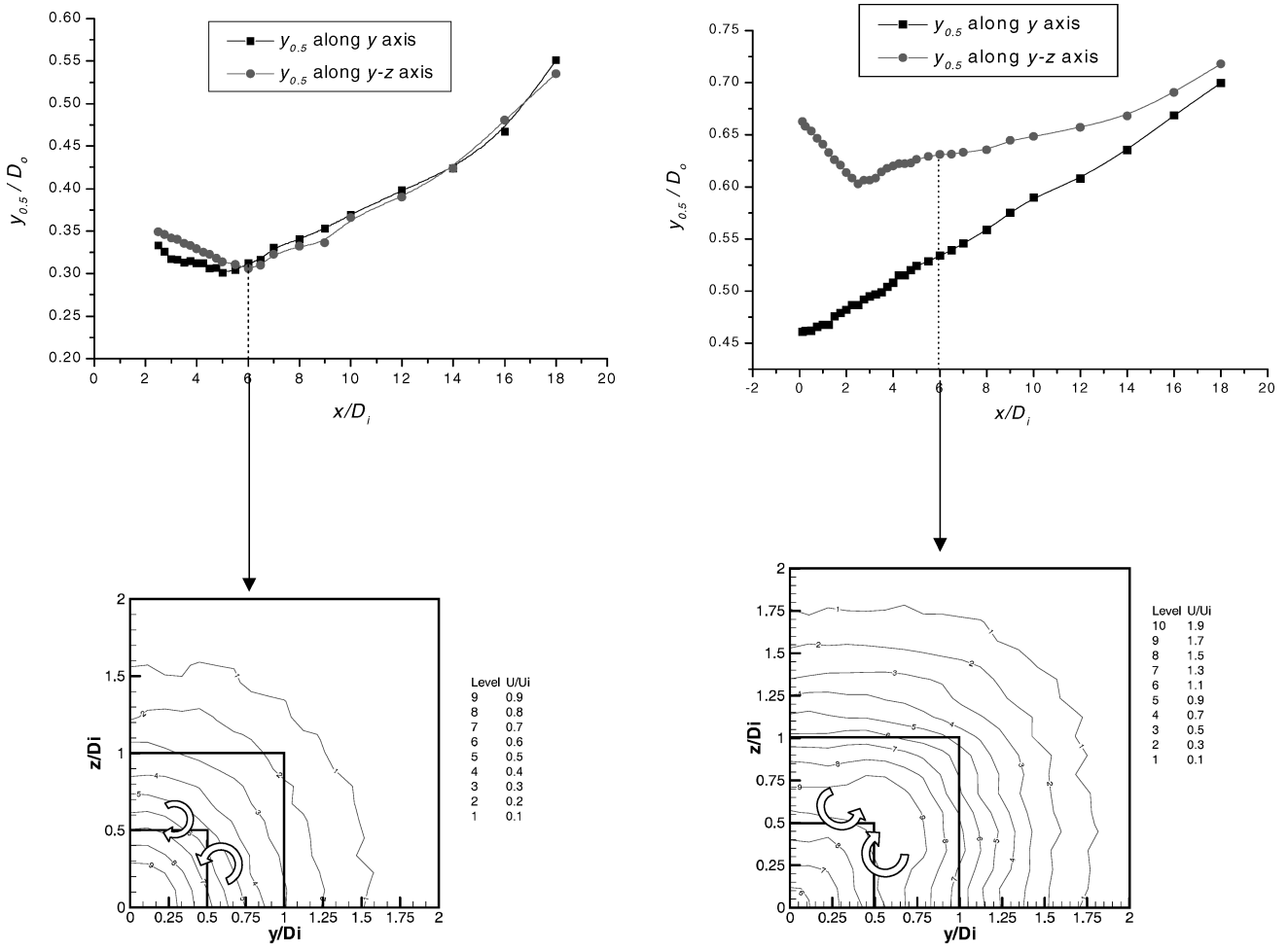

a) $\gamma_u = 0.5$ **b) $\gamma_u = 2.0$**

Fig. 9 Development of half-width $y_{0.5}$ along the *y* and *y–z* axes.

among the three cases at about $0.18U_i$. The lateral velocities tend to persist until about $x/D_i = 10$ (not shown here). In the case of a square jet with triangular mixing tab attached,[18] the maximum strength of the secondary flow velocities immediately behind the tab was at about $0.30U_i$ and is some 30% higher than the vortices that are naturally formed.

At locations farther downstream and for the smallest velocity ratio of $\gamma_u = 0.5$ (Figs. 5a and 5b), the outer potential core decayed faster, and the outer and inner mixing layers merged smoothly, forming a Gaussian velocity profile as early as at $4D_i$. For velocity ratio $\gamma_u = 2.0$ and Figs. 6a and 6b, it takes a longer distance for the outer jet to entrain the low inner jet-exit fluid, and a Gaussian jet velocity profile can only be identified at about $12D_i$.

E. Reynolds Normal and Shear Stresses Along the *y*-Axis

For the streamwise and lateral rms velocities for cases $\gamma_u = 0.5$ and $\gamma_u = 2.0$, two peaks can be found at stations close to the jet exit (Figs. 7a and 7b and 8a and 8b). The inner two correspond to the inner mixing layer, and the outer two correspond to the outer mixing layer. As the velocity ratio increases, the maximum of normalized rms velocity also increases, that is, $(u'/U_i)_{\max} = 0.1$, 0.2, and 0.35, for $\gamma_u = 0.5$, 1.0 and 2.0, respectively. This clearly shows the rms velocities are closely related to the shape of the streamwise mean velocity profiles, as one would expect from the production terms in the turbulent kinetic energy equation. Notice also that the maximum rms velocity at $\gamma_u = 0.5$ has the lowest value and the velocity ratio of $\gamma_u = 2.0$ has the highest maximum. At $\gamma_u = 0.5$, the rms velocity of the inner jet is higher than the outer jet, whereas for $\gamma_u = 1.0$ and 2.0 the rms velocity of the outer jet is persistently higher than those of the inner jet within the range of measurement. The magnitude of the rms velocities across the jet dropped at stations farther downstream.

Similarly, for the Reynolds shear-stress distribution for cases $\gamma_u = 0.5$ and 2.0 (Figs. 7b and 8b), the dependence on the streamwise mean velocity gradients and the extent of the potential cores are evident.

F. Vortex Dynamics in the Near Field of a Coaxial Square Jet

Because of the azimuthal nonuniformities inherent in a square-shaped nozzle, downstream developments for the velocity profiles along the y and y–z axes (as shown in Fig. 1) would be different. As a result of the corner vortex formation, the phenomenon of axis switching at the downstream locations[10] can be caused. Chua et al.[16] have investigated the axis switching of a single square jet issuing into stagnant environment and found that there is an axis switching at about $4D_e$, whereas Quinn[10] observed that the switching occurred at about $1.25D_e$ for a sharp-edged single square nozzle.

To examine this effect, half-width $y_{0.5}$ was evaluated from measurements taken along the axis perpendicular to the sides (y direction) and along the diagonal (y–z direction) for the respective cases. $y_{0.5}$ is defined as the position where $U = 0.5U_{\max}$, in which $U_{\max}$ is the maximum value along the transverse plane. Figure 9 shows the growth of the half-width along the y and x–y directions with the streamwise distance. As shown, no obvious axes-switching phenomenon was found for the three cases. It, however, shows that the two curves merged at about $x/D_i = 4.3$ for $\gamma_u = 1.0$, whereas for the other two cases (Figs. 9a and 9b), the two curves merged at about $5D_i$ and beyond $18D_i$ for $\gamma_u = 0.5$ and 2.0, respectively.

Selective streamwise mean velocity contours for respective cases are also shown in Fig. 9 (inset). For $\gamma_u = 1.0$, the merging of the two curves at about $x/D_i = 4.3$ appeared to be affected by the generation of the corner streamwise vortices at the inner jet. The outer jet did not seem to have exerted the same influence. This can be further confirmed by the measurements of the lateral velocities at the corresponding region, which did not reveal any flow recirculation at around the corner of the outer nozzle wall. For $\gamma_u = 0.5$, similar to that found in the $\gamma_u = 1.0$, velocity contours show that the generation of the corner streamwise vortices appeared only around the inner nozzle. As a result, the contours at around the inner nozzle wall were seen to migrate toward the jet centerline (Fig. 9a). There is also some differences in terms of streamwise vortex strength for the two cases; maximum lateral velocities are $0.09U_i$ and $0.05U_i$ for

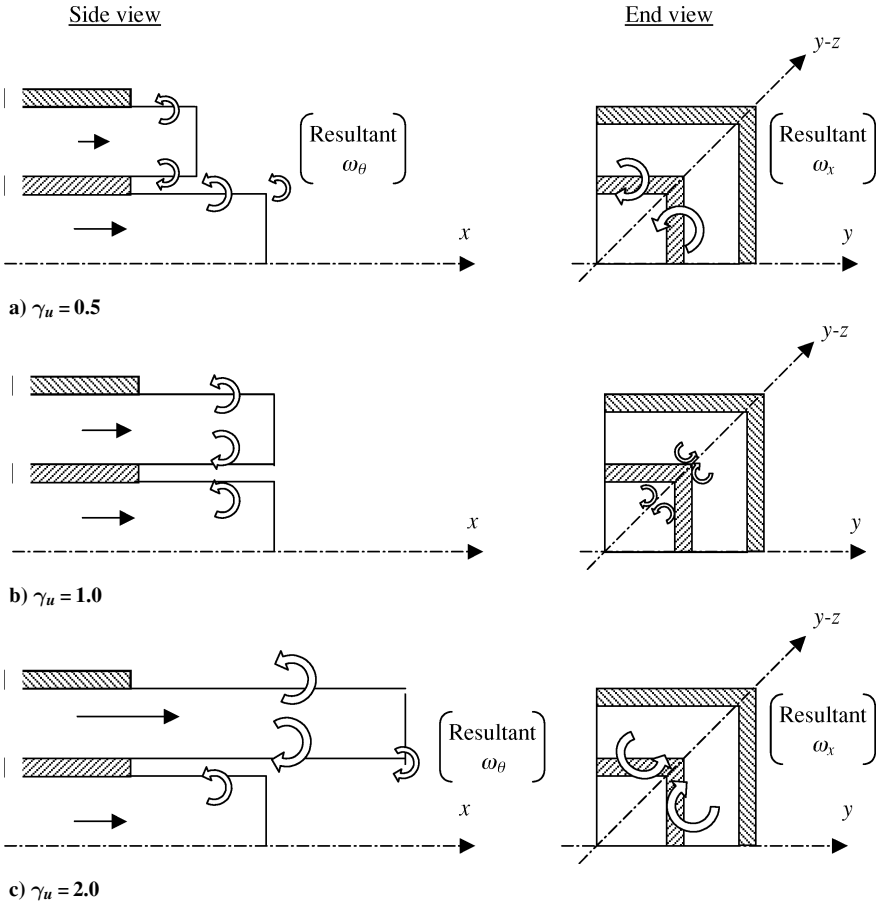

Fig. 10 Schematic of the vortex dynamics in the coaxial square jet for the three velocity ratios.

$\gamma_u = 0.5$ and 1.0, respectively. The presence of the streamwise vortices have enhanced mixing between the two streams and can also explain the fast merging of the half-widths as early as $x/D_i = 4.3$.

For $\gamma_u = 2.0$ in which the inner nozzle has a higher velocity, the distribution of the contours at around the inner nozzle is very different from the other two cases (Fig. 9b). In contrast to the other two cases, the contours are being pushed away from the centerline along the y–z direction as a result of the opposite sense of rotation for the streamwise vortices. The strength of the streamwise vortices is also relatively stronger than the other two cases shown earlier (maximum at about $0.2U_i$), and a longer distance is required for them to decay down to a negligible level.

As shown schematically in Fig. 10, at different velocity ratios, the direction of the resultant vortex ring formed immediately behind the trailing edge of the inner jet would achieve different sense of rotation.[11] For $\gamma_u = 0.5$ and 2.0, as shown in Figs. 10a and 10c, the direction of the resultant vortex ring generated would be different in both the sense of rotation and strength (as indicated by the size of the arrows). In our experiment, the velocity of the inner jet is fixed. As such, the outer vortex ring would be the strongest for $\gamma_u = 2.0$ (Fig. 10c). For $\gamma_u = 0.5$, the presence of these corner vortices facilitated the merging of the two axes. In contrast, for $\gamma_u = 2.0$, the streamwise vortices had stronger strength and developed an opposite sense of rotation, relative to the other two cases, and hence spreading the inner jet radially outward along the y–z axis direction. The obvious result is that the two axes did not merge until after $x/D_i = 18$.

Figure 11 shows the development of normalized volume flux with downstream distance for respective cases. As might have been expected, $\gamma_u = 2.0$ has the fastest growth rate and is followed by $\gamma_u = 1.0$ and 0.5. This can be explained by the fact that the direction of the streamwise vortices found in $\gamma_u = 0.5$ did not facilitate the spreading the jet to the surroundings (cf., Fig. 10a).

For all three of the cases, the streamwise vortices did not appear at the corner of the outer jet. The only plausible reason is that as the initial vortex ring emerged from the jet-exit plane some of its strength was dissipated through entrainment of the surrounding fluids. In contrast, for the case of an orifice exit the vena contracta region tends to strengthen the vortex ring that emerges. This can probably explain why the square jet discharged from a sharp-edged orifice can achieve faster axis switching (cf., Fig. 4a). Moreover, it is important to point out that the presence of the corner streamwise vortices did not necessarily lead to the onset of axis switching, but they did enable the mixing, at least in the mean sense, to be achieved faster. This is clearly shown in the similarity comparison for the mean and rms velocities earlier.

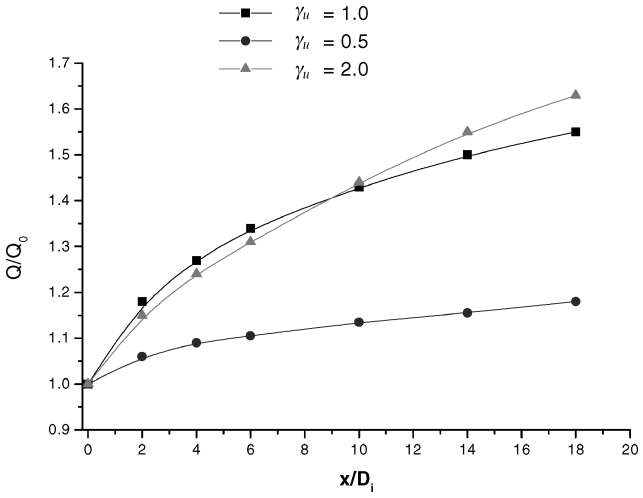

Fig. 11 Development of normalized cross-sectional volume flux Q/Q_o with downstream distance for the three cases considered.

IV. Conclusions

This study presents some global characteristics of the coaxial square jet (with fixed inner initial velocity) at three different velocity ratios, that is, $\gamma_u = U_o/U_i = 0.5$, 1.0, and 2.0. The results show that the inner potential core length x_{pi} is greatly affected by the velocity ratio γ_u but the outer potential core length x_{po} increases slightly as γ_u is increased. These trends are very similar to those found in a circular coaxial jet, but the extent of the potential core is at least one inner diameter shorter than the circular coaxial jet under similar flow conditions.

Case $\gamma_u = 0.5$ has achieved the largest spreading rate among the three cases considered. The spreading rates for the three cases are generally faster than their circular counterpart. Of particular note is that the spreading rate for $\gamma_u = 0.5$ was initially lower than the case for the coaxial circular jet with swirl but eventually caught up and eventually overtook it in the far field. It is certain that the presence of the corner streamwise vortices would enhance the mixing between the two coflowing streams and that with the surrounding fluid medium at a faster rate and at a finer scale than their circular counterparts.

Acknowledgments

Financial support to this project from the Academic Research Committee and the graduate scholarship for X. K. Wang from the School of Mechanical and Production Engineering are gratefully acknowledged.

References

[1]Forstall, W., and Shapiro, A. H., "Momentum and Mass Transfer in Co-Streamwise Gas Jets," *Journal of Applied Mechanics*, Vol. 101, 1950, pp. 521–529.

[2]Champagne, F. H., and Wygnanski, I. J., "An Experimental Investigation of Coaxial Turbulent Jets," *International Journal of Heat and Mass Transfer*, Vol. 14, 1971, pp. 1445–1464.

[3]Durao, D. F. G., and Whitelaw, J. H., "Turbulent Mixing in the Developing Region of Coaxial Jets," *Journal of Fluids Engineering*, Vol. 95, 1973, pp. 467–473.

[4]Ribeiro, M. M., and Whitelaw, J. H., "Co-Axial Jets with and Without Swirl," *Journal of Fluid Mechanics*, Vol. 96, 1980, pp. 769–795.

[5]Buresti, G., Talamelli, A., and Petagna, P., "Experimental Characterization of the Velocity Field of a Coaxial Jet Configuration," *Experimental Thermal and Fluid Science*, Vol. 9, 1994, pp. 135–146.

[6]Ko, N. W. M., and Au, H., "Coaxial Jets of Different Mean Velocity Ratios," *Journal of Sound and Vibration*, Vol. 100, 1985, pp. 211–232.

[7]Rehab, H., Villeramux, E., and Hopfinger, E. J., "Flow Regimes of Large Velocity Ratio Coaxial Jets," *Journal of Fluid Mechanics*, Vol. 345, 1997, pp. 357–381.

[8]Villeramux, E., and Rrehab, H., "Mixing in Coaxial Jets," *Journal of Fluid Mechanics*, Vol. 425, 2000, pp. 161–185.

[9]Yu, S. C. M., and Xu, X. G., "Flow Characteristics of Confined Coaxial Nozzle Flow with a Central Lobed Mixer at Different Velocity Ratios," *AIAA Journal*, Vol. 36, 1998, pp. 349–358.

[10]Quinn, W., "Streamwise Evolution of a Square Jet Cross-Section," *AIAA Journal*, Vol. 27, 1992, pp. 2853–2857.

[11]Gutmark, E. J., and Grinstein, F. F., "Flow Control with Non-Circular Jets," *Annual Review of Fluid Mechanics*, Vol. 31, 1999, pp. 239–272.

[12]Grinstein, F. F., Gutmark, E., and Parr, T., "Near Field Dynamics of Subsonic Free Square Jets: A Computational and Experimental Study," *Physics of Fluids*, Vol. 7, 1995, pp. 1483–1497.

[13]Au, H., and Ko, N. W. M., "Coaxial Jets of Different Mean Velocity Ratios (Part 2)," *Journal of Sound and Vibration*, Vol. 116, 1987, pp. 427–443.

[14]Bitting, J. W., Nokitopoulos, D. E., Gogineni, S. P., and Gutmark, E. J., "Visualization and Two-Color DPIV Measurements of Flows in Circular and Square Coaxial Jets," *Experiments in Fluids*, Vol. 31, 2001, pp. 1–12.

[15]Mi, J., Nathan, G. J., and Luxton, R. E., "Centre-Line Mixing Characteristics of Jets from Nine Different Shaped Nozzles," *Experiments in Fluids*, Vol. 28, 2000, pp. 93, 94.

[16]Chua, L. P., Li, Y. F., Yu, S. C. M., and Zhou, T., "Axis-Switching of a Square Jet," *Proceedings of 14th Australasian Fluid Mechanics Conference*, 2001.

J. P. Gore
Associate Editor